JACS
JOURNAL OF THE AMERICAN CHEMICAL SOCIETY
Article
pubs.acs.org/JACS

What Makes the Photocatalytic CO_2 Reduction on N-Doped Ta_2O_5 Efficient: Insights from Nonadiabatic Molecular Dynamics

Alexey V. Akimov,[†] Ryoji Asahi,[‡] Ryosuke Jinnouchi,[‡] and Oleg V. Prezhdo*[,†]

[†]Department of Chemistry, University of Southern California, Los Angeles, California 90089, United States
[‡]Toyota Central Research and Development Laboratories, Inc., 41-1 Yokomichi, Nagakute-shi, Aichi 480-1192, Japan

Supporting Information

ABSTRACT: Recent experimental studies demonstrated that photocatalytic CO_2 reduction by Ru catalysts assembled on N-doped Ta_2O_5 surface is strongly dependent on the nature of the anchor group with which the Ru complexes are attached to the substrate. We report a comprehensive atomistic analysis of electron transfer dynamics in electroneutral Ru(di-X-bpy)$(CO)_2Cl_2$ complexes with X = COOH and PO_3H_2 attached to the N−Ta_2O_5 substrate. Nonadiabatic molecular dynamics simulations indicate that the electron transfer is faster in complexes with COOH anchors than in complexes with PO_3H_2 groups, due to larger nonadiabatic coupling. Quantum coherence counteracts this effect, however, to a small extent. The COOH anchor promotes the transfer with significantly higher frequency modes than PO_3H_2, due to both lighter atoms (C vs P) and stronger bonds (double vs single). The acceptor state delocalizes onto COOH, but not PO_3H_2, further favoring electron transfer in the COOH system. At the same time, the COOH anchor is prone to decomposition, in contrast to PO_3H_2, making the former show smaller turnover numbers in some cases. These theoretical predictions are consistent with recent experimental results, legitimating the proposed mechanism of the electron transfer. We emphasize the role of anchor stability, nonadiabatic coupling, and quantum coherence in determining the overall efficiency of artificial photocatalytic systems.

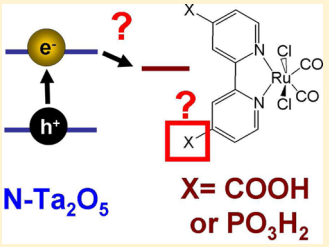

1. INTRODUCTION

Harvesting and transformation of solar energy by artificial photosynthetic complexes[1−6] is one of the most important challenges of modern chemistry. The availability of suitable materials[7−14] that can effectively collect solar photons and transform them into electrical or chemical energy opens attractive prospects to renewable and clean energy supply and production of basic chemicals. In particular, photocatalytic carbon dioxide reduction to low-carbon organic molecules, such as formic acid or carbon monoxide, has been attracting interest of many research groups over the last decades.[2,15−23] Carbon dioxide capture is also an important technology for air pollution and climate change control.[16,18] Although the advances in synthesis and experimentation have suggested many practical routes to better materials for CO_2 reduction, the fundamental mechanisms of the processes that occur at different stages of CO_2 reduction are not completely understood. In particular, interactions at the catalyst−substrate interface play one of the most important roles, as has been suggested by numerous studies.[24−33] Yet, there is still significant controversy in attributing observed efficiencies to particular atomic-scale mechanisms.

Ru complexes have been utilized for many years in various photoconversion applications, including water splitting,[34−36] electricity generation with dye-sensitized solar cells,[37−40] and CO_2 reduction.[23,41,42] In recent experiments of Sato and co-workers,[41,42] Ru complexes attached to an N-doped Ta_2O_5 (N−Ta_2O_5) substrate have been studied as promising photocatalysts for CO_2 reduction. The experimental observations suggested that anchor groups, which bind Ru complexes to the semiconductor, have a very pronounced effect on the reduction efficiency, as judged by the turnover numbers (TONs). Increasing the number of carboxyl groups in the Ru ligands increases TONs, as demonstrated in a series of Ru complexes: $[Ru(bpy)_2(CO)_2]^{2+}$, [Ru(dcbpy) (bpy) $(CO)_2]^{2+}$, and $[Ru(dcbpy)_2(CO)_2]^{2+}$, where bpy and dcbpy refer to 2,2′-bipyridyne and 4,4′-dicarboxy-2,2′-bipyridyne ligands, respectively. The observed TONs correlate with the driving force for the electron transfer (ET) in the corresponding systems and with the number of COOH groups that can act as anchors. The effect can naturally be attributed to energetic factors as well as to enhanced charge transfer fluxes due to the increased number of anchor groups.

Complementing the work of Sato and co-workers,[41,42] Suzuki et al.[43] varied the nature of the anchor group. They studied [Ru(dcbpy) (bpy) $(CO)_2]^{2+}$ and [Ru(dpbpy) (bpy) $(CO)_2]^{2+}$, where dpbpy refers to 4,4′-diphosphonate-2,2′-bipyridyne, attached to a N−Ta_2O_5 substrate. The two systems differ only in the substituent groups in disubstituted bipyridyne ligands. The experimentally measured driving forces for the two systems are comparable to each other, and the apparent number of anchor groups per Ru complex is same for the two systems. Yet, the observed TONs are strikingly different: they are much larger for the catalyst attached with the PO_3H_2 anchor than with COOH. Both studies clearly indicate that

Received: July 16, 2015
Published: August 19, 2015

DOI: 10.1021/jacs.5b07454
J. Am. Chem. Soc. 2015, 137, 11517−11525

anchoring groups play a dominating role. However, the fundamental reasons behind these experimental observations are unclear, strongly motivating the need for explicit atomistic computational studies.

In the present work, we report important insights into the photoinduced ET mechanisms, which determine the role of the anchor group. We utilize atomistic nonadiabatic molecular dynamics (NA-MD) in order to obtain a detailed time-domain description of ET in N−Ta_2O_5 sensitized with Ru complexes. Following our earlier work,[44] we utilize the electroneutral Ru(di-X-bpy) $(CO)_2Cl_2$ complexes with X = COOH and PO_3H_2 attached to N−Ta_2O_5. We show that the COOH anchor leads to a larger nonadiabatic coupling (NAC) between the N−Ta_2O_5 donor and the Ru-complex acceptor, facilitating faster ET. Our analysis suggests that quantum coherence favors faster ET in the PO_3H_2 system, but its role is less than that of the NAC. We present the rationale for these two opposing effects, based on the analysis of electronic structure and electron-vibrational coupling in the two systems.

Our calculations provide a rather surprising conclusion that the intrinsic ET process is faster in the COOH system than in the PO_3H_2 system, in contrast to the trends in the previously reported experimental TONs. We argue that, despite the contrast with the experiment, there are good reasons why our results are qualitatively correct, including the agreement with other related studies, both experimental and computational. As such, our results also suggest that the factors other than ET rates can be behind the observed trends in the measured TONs. The other factors may include surface effects, such as varying effective coverage due to desorption, decomposition, and reduction of the adsorbed Ru complexes with COOH anchors.

2. METHOD

2.1. Processes and Techniques. We address the relationship of interfacial ET between N−Ta_2O_5 and Ru complexes to the nature of the anchor groups with which the Ru complexes are attached to the substrate. The process of interest is depicted schematically in Figure 1.

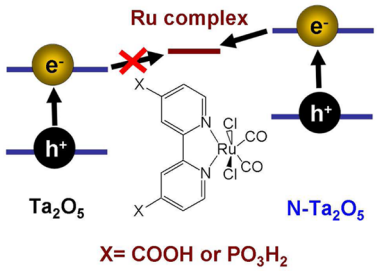

Figure 1. Conceptual scheme of studied processes. ET from N-doped Ta_2O_5 (N−Ta_2O_5) to Ru complex bound to the N−Ta_2O_5 substrate via one of the two anchor groups: X = COOH or PO_3H_2. ET from undoped Ta_2O_5 is prohibited energetically.

N−Ta_2O_5 acts as a chromophore by absorbing light, which excites electrons and promotes them from the occupied valence band (VB) levels to the unoccupied conduction band (CB) levels. The photoexcited electrons can be injected from the N−Ta_2O_5 subsystem to the lowest or next lowest unoccupied molecular orbitals (LUMO or LUMO+n) of the Ru catalyst adsorbed on the surface, as long as the energy of the acceptor states is below the energy of the donor states (Figure 1, right). The injected electron is used in the CO_2 reduction reactions.

In our recent work,[44] we investigated the electronic structure of Ru complexes attached to the pure Ta_2O_5 substrate with OH, COOH, and PO_3H_2 anchors. We found that the alignment of the energy levels in Ta_2O_5 and Ru complexes was not favorable for the ET to occur, because the acceptor level was higher in energy than the donor level (Figure 1, left). N-Doping was suggested as one of the most critical factors making the ET possible. Recent, yet unpublished data of Jinnouchi et al.[45] confirm the calculation results. The authors showed that the CB edge is shifted toward more positive energies, when Ta_2O_5 is doped with N atoms. The atomistic origin of such shift was attributed to electrostatic effects due to the dipole created by the N−O layer in the doped material.

In the present work, we take the previously developed methodology to the state-of-the-art level, by performing NA-MD simulations. The approach combines classical molecular mechanics (MM) and extended Hückel theory (EHT) to compute nuclear dynamics and electronic structure, respectively. The MM part is used to produce well-thermalized and sufficiently long ground state molecular dynamics (MD) trajectories. The EHT gives the electronic structure, including both energy levels and NAC, for each point along the trajectories. The electronic structure information is subsequently used to perform NA-MD simulations within the classical path approximation that neglects electron back-reaction on the nuclear dynamics. We use the results of the NA-MD calculations to analyze and compare the ET dynamics in the COOH and PO_3H_2 systems.

2.2. Molecular Structure and Dynamics. The molecular models used in the present work are depicted in Figure 2. Following the

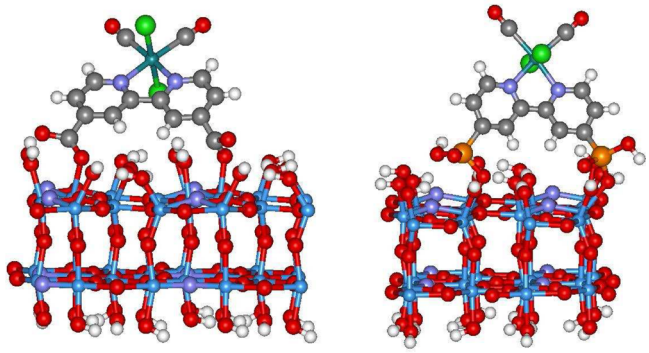

Figure 2. Molecular structures used in the present calculations: Ru-complexes attached to N−Ta_2O_5 clusters via COOH (a) and PO_3H_2 (b) anchors.

stability considerations, we assume that Ru complexes are bound via two anchor groups. The hydroxyl groups of the N−Ta_2O_5 surface binding the anchors are chosen to mimize distortion of the adsorbate. Because of different flexibility of the anchors, the resulting bound complexes differ in relative orientation of the Ru complex and substrate. Although the coordination mode can, in principle, affect the nonadiabatic couplings and electronic energy levels of a system, this effect is rather minimal for our complexes. As we have demonstrated in the previous work, both mono- and bidentate coordination of the PO_3H_2 anchor result in practically indistinguishable pDOS. For the COOH anchor, the bidentate binding may create defect states. However, the presence of such states will only enhance charge transfer to COOH complex. As we will show below, defects will not change the qualitative results obtained in this work. We used a 10% doped cluster of Ta_2O_5, which is close to the 8.9% nitrogen content in the experiments.[46]

In view of the need for expensive evaluation of electronic structure at each point of the MD trajectories, we utilize a minimal N−Ta_2O_5 cluster, yet sufficiently large to adequately represent the surface. Molecular structures as well as MD trajectories are computed using our implementation of the rigid-body molecular dynamics (RB-MD), with highly accurate and stable qTerec algorithm.[47] The coordinates of

DOI: 10.1021/jacs.5b07454
J. Am. Chem. Soc. 2015, 137, 11517−11525

the optimized geometries of the two complexes are presented in the Supporting Information.

In the RB-MD, one constrains arbitrary degrees of freedom via grouping specific atoms in united fragments. The nuclear dynamics of the system is then described in terms of translations and rotations of the rigid bodies into which the system is partitioned. In the limiting case, a single atom can be considered a rigid fragment with fully degenerate rotational degrees of freedom. Currently, we focus solely on the role of the anchor, and therefore, treat the entire Ru complex and the cluster representing the N−Ta_2O_5 surface as two distinct rigid fragments. The anchor groups are fully flexible at the atomistic level. Hence, the Ru-complex/N−Ta_2O_5 system with the COOH is composed of 8 fragments, 6 of which are the atoms of two −COO groups, and the PO_3H_2 system is composed of 12 fragments, 10 of which are the atoms of two −PO_3H groups. The geometry of the N−Ta_2O_5 cluster and Ru complexes are taken from our previous calculations[44] performed using the hybrid functional of Heyd, Scuseria, and Ernzerhof (HSE06). The interactions between all rigid bodies are computed based on the explicit-atom universal force field, UFF.[48] As any other force fields, UFF would predict the structures of Ru complex and N−Ta_2O_5 to be different from the DFT-optimized structures. The rigid-body approach helps us to avoid any spurious effects due to structural differences. At the same time, the all-atomic description of the anchor groups allows us to focus on the ET dynamics through the anchors and to reveal the factors that stem only from their nature.

We optimize the COOH and PO_3H_2 systems by several rounds of simulated annealing. Each round consists of 100−200 cycles. Each cycle consists of a short MD simulation (1−100 fs), followed by resetting all linear and angular momenta of moving rigid fragment to zero. Initial annealing rounds utilize 0.1 fs integration timesteps. The subsequent rounds utilize larger, 1 fs, integration timesteps. Once the system is annealed until the heat production is negligible, we thermalize the system by running a 25 ps MD simulation in the NVT ensemble with the target temperature of 278 K. Temperature is maintained by the Nose-Hoover chain thermostat[49,50] of length 3. The 25 ps thermalization period is followed by the 5 ps production run. The obtained trajectories are used to compute coordinate-dependent vibronic Hamiltonians needed for NA-MD simulations.

2.3. Electronic Structure. The electronic structure calculations are performed using our implementation of the semiempirical EHT method.[51−53] EHT utilizes a minimal basis set of atomic s, p, and d orbitals. The matrix elements of the electronic Hamiltonian, H_{el}, are defined as $(H_{el})_{ij} = K_{ij}((I_i + I_j)/2)S_{ij}$, where I_i are the atomic orbital energies, routinely set to negative of the valence state ionization potentials, K_{ij} is a proportionality factor that may, in principle, depend on orbital types, and S_{ij} is the overlap of atomic orbitals.

The use of EHT is essential for efficient computations with the systems of interest: the N−Ta_2O_5 cluster contains many Ta atoms, each contributing many electrons and orbitals. Thus, the electronic structure calculations quickly become expensive even for small clusters. Keeping in mind that such calculations must be done for many configurations along the MD trajectory, and that NAC matrices must be computed as well, the computational expenses become unfeasible for standard ab initio or DFT methods. At the same time, the tight-binding theories, including EHT, are well-known for capturing essential physics,[54−56,38,57−65] which makes them reliable and transparent for qualitative analysis of chemical phenomena.

Although EHT is a well-defined tight-binding method, it lacks explicit electrostatic effects.[66] The effects can be included in a more elaborate self-consistent charge version[67−69] or using a configuration-interaction approach,[65] but the costs would increase by at least an order of magnitude due to the need for self-consistency iterations or multiple configurations, respectively. Therefore, in the present work we choose to develop an effective parametrization that would capture the shift of the CB minimum level in N-doped Ta_2O_5, placing this level above the acceptor levels of the Ru complexes.

For the EHT parametrization, we utilize a set of three Ru complexes with different anchor groups, as well as moderate-size N−Ta_2O_5 clusters. The parametrization includes variation of the orbital energies, I_i, the proportionality constants, K_{ij}, and the atomic orbital exponents. The parametrization is performed to reproduce the absolute values of the frontier occupied and unoccupied orbitals in all four training systems. The target values for the conduction band minimum (CBM) and valence band maximum (VBM) of N−Ta_2O_5 are taken from the experiment: The values reported from ultraviolet photoelectron spectroscopy (UPS)[41] and those measured electrochemically in solution,[46] are close to each other. The HOMO/LUMO energy levels of the Ru complexes obtained in our earlier HSE06 calculations[44] are used as the reference values. Ideally, the target values should be obtained from experimental measurements. However, such data are not available for the Ru(di-X-bpy) $(CO)_2Cl_2$ complexes used in the present work. At the same time, the values for other complexes such as $[Ru(dcbpy)\ (bpy)\ (CO)_2]^{2+}$ and $[Ru(dpbpy)\ (bpy)\ (CO)_2]^{2+}$ agree well with the corresponding HSE06 results. However, we observe a systematic difference in these values, on the order of 0.2 eV. This difference is used as a correction to adjust the computed HOMO/LUMO levels of Ru(di-X-bpy) $(CO)_2Cl_2$ to estimate the expected experimental values. These corrected energies are used in our EHT parametrization as the reference values. Table 1 summarizes the frontier orbital energy levels of the training set system computed with the optimized EHT parameters and the corresponding reference values. The optimized EHT parameters are provided in the Supporting Information, section A. Further we shall discuss the orbitals of our primary interest: the LUMO levels of the Ru complexes and the CBM of N−Ta_2O_5.

Table 1. LUMO/CBM Energy Levels for the Ru-(di-X-bpy) $(CO)_2Cl_2$ Complexes and N−Ta_2O_5 Used in Parameterization

system	computed, eV	HSE06 (*) or experiment (**), eV
X = COOH	−3.79	−3.58*
X = PO_3H_2	−3.51	−3.52*
X = OH	−3.33	−2.92*
N−Ta_2O_5	−2.78	−2.8**

The agreement in the absolute values of the computed and target CBM levels of the N−Ta_2O_5 cluster is very good, thanks to the sufficient number of degrees of freedom used in the parametrization. The agreement in the absolute values for the three Ru complexes is satisfactory, showing some deviations from the corresponding target values for the OH and COOH systems. The deviations are modest. More importantly, the absolute values are less critical for our purposes. What matters the most, is that the two main qualitative features are captured well. First, the EHT calculations reproduce the monotonous increase of the energy levels in a series COOH < PO_3H_2 < OH, which is also observed for the adjusted HSE06 values. Second, the CBM energy of the N−Ta_2O_5 cluster is higher than the LUMO (and also LUMO+1, for COOH) energy levels of isolated Ru complexes. Proper energy level alignment, reproduced by EHT, is essential for making the interfacial ET possible. We emphasize again that this favorable energy level alignment originates from the N-doping of Ta_2O_5, and it is not observed in pure Ta_2O_5.

As it was shown in our previous work,[44] the donor and acceptor energy level alignment present in free components (unbound Ru complex and substrate) is well preserved in the bound systems. Nonetheless, this effect needs explicit verification, especially when a new parameter set is developed. To verify that the alignment is preserved in the bound complexes, we compute the projected density of state (pDOS) for each system, shown in Figure 2. We project the DOS on the sets of atoms that constitute the Ru complex together with the anchor and the N−Ta_2O_5 substrate. The results are shown in Figure 3. One can observe that there are two unoccupied acceptor levels (LUMO and LUMO+1) below the N−Ta_2O_5 CBM in the COOH system (Figure 3a), and there is only one such level (LUMO) in the PO_3H_2 system (Figure 3b). The energy level alignment in the bound systems is consistent with that in the unbound components, suggesting that the present parametrization is suitable for modeling the ET dynamics in the bound system.

DOI: 10.1021/jacs.5b07454
J. Am. Chem. Soc. 2015, 137, 11517−11525

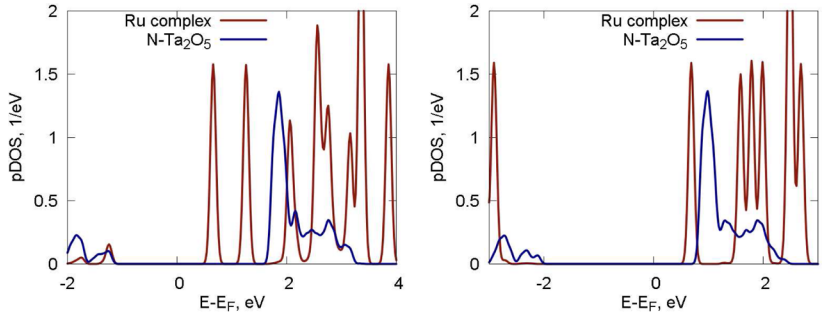

Figure 3. PDOS computed for the (a) COOH and (b) PO_3H_2 systems. The pDOS of the N−Ta_2O_5 is decreased by the factor of 50, for clarity.

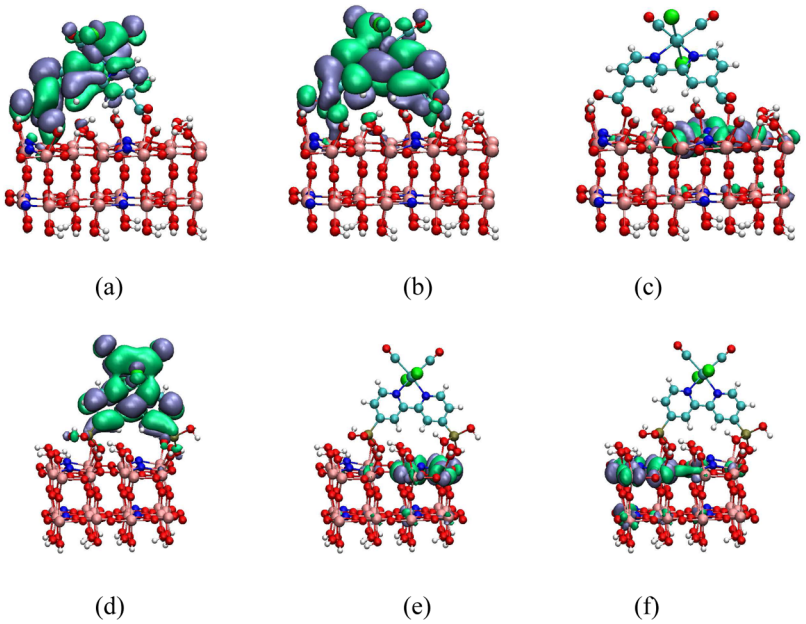

Figure 4. Frontier orbitals involved in the charge transfer: LUMO (a, d), LUMO+1 (b, e), and LUMO+2 (c, f). Top and bottom row corresponds to orbitals of Ru complex with COOH and PO_3H_2 anchors, respectively. The isosurface magnitude is 0.01 $bohr^{-3}$.

2.4. Nonadiabatic Molecular Dynamics. To carry out nonadiabatic ET simulations, we utilize the PYXAID code[70,71] designed for modeling of NA-MD in nanoscale systems. In the NA-MD simulations, we first solve the time-dependent Schrödinger equation (TD-SE), $i\hbar(\partial\Psi/\partial t) = H\Psi$, where $H = T_{nucl} + H_{el}$ is the total Hamiltonian of the system. The overall electron−nuclear wave function, Ψ, is represented as a superposition of electronic basis states, $|i\rangle$, weighted by the time-dependent coefficients, $c_i(t)$: $\Psi = \Sigma_i c_i(t)|i\rangle$. The electronic basis states $|i\rangle$ can, in principle, be chosen arbitrarily. In the present work, we utilize a set of Slater determinants[70,71] constructed from the adiabatic MOs of the bound Ru-catalys/N−Ta_2O_5 complexes. The TD-SE in the basis of electronic states reduces to the semiclassical TD-SE: $i\hbar(\partial c_i(t)/\partial t) = \Sigma_i(H_{vib})_{i,j}\, c_j(t)$, where H_{vib} is the vibronic (electron−nuclear) Hamiltonian, defined in terms of state energies, E_i and NAC for pairs of states, $D_{ij} = \langle i|(\partial/\partial t)|j\rangle$, as following: $(H_{vib})_{i,j} = E_i\delta_{ij} - i\hbar D_{ij}$. The energies E_i are computed by diagonalizing the electronic EHT Hamiltonian: $H_{el}C = SCE$, where C is the matrix of MO-LCAO coefficients and S is the matrix of AO overlaps. The energies and NAC needed to construct the vibronic Hamiltonian are computed in our composite MD//EHT scheme, described in the previous sections.

Solution of the semiclassical TD-SE does not account for detailed balance, allowing barrier-less access to high-energy states from any arbitrary initial state. The electron-vibrational energy relaxation taking place during the ET process is mistreated, and thermodynamic equilibrium cannot be achieved in the long-time limit. To remedy this problem, we use the obtained coefficients, $c_i(t)$, only as auxiliary quantities for the fewest switches surface hopping (FSSH) NA-MD algorithm.[72] In the FSSH, a swarm of trajectories is propagated, and each trajectory may diffuse in the Hilbert space of electronic basis states included in the model. The hopping probabilities depend on the semiclassical TD-SE amplitudes, $c_i(t)$, as well as on the NAC between source and target states, $D_{source,target}$. The averaging over all stochastic realizations of the FSSH trajectories and over all initial conditions (different starting configurations) yields SH populations of different states: $P_i(t) = \langle N_i(t)/N_{tot}\rangle$, where $\langle\rangle$ denotes thermal averaging. For more details on the NA-MD method and its trajectory surface hopping implementation, we refer the reader to the original works[70−72] and related review papers.[73−77]

We are interested in the dynamics of population transfer from the donor states localized on N−Ta_2O_5 to the acceptor states of the Ru complexes. This goal determines the choice of the model space of electronic basis states (the active apace). The classification of electronic states of the combined Ru-complex/N−Ta_2O_5 systems as either donor or acceptor is based on the analysis of the pDOS shown in Figure 3. The COOH system contains two Ru-complex levels below the N−Ta_2O_5 CB (Figure 3a). These are the LUMO and LUMO+1 states of the bound complex. These are electron acceptor states. In the case of the PO_3H_2 system, there is only one state below the CB of N−Ta_2O_5 (Figure 3b). Thus, only LUMO is assigned as an acceptor state

DOI: 10.1021/jacs.5b07454
J. Am. Chem. Soc. 2015, 137, 11517−11525

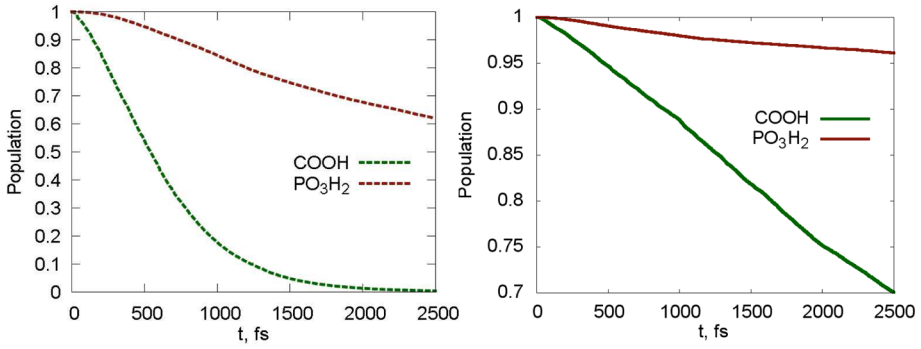

Figure 5. Decay of the total population of donor ($N-Ta_2O_5$) states. Results for COOH and PO_3H_2 anchors are present: (a) without decoherence and (b) with decoherence.

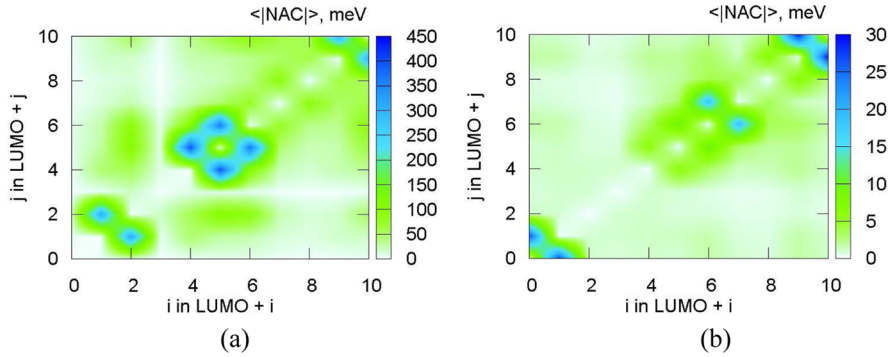

Figure 6. Visualization of the NACs between unoccupied orbitals of $N-Ta_2O_5$ and Ru complex attached via either COOH anchor (a) or PO_3H_2 anchor (b). NAC values at noninteger points are interpolated from the values at integer-valued x and y coordinates.

for this system. For both systems we choose a set of states localized on $N-Ta_2O_5$. LUMO+n through LUMO+n+m (n = 3 for COOH; and n = 2 for PO_3H_2; $n + m = 10$) to act as donor states. These states span approximately a 1 eV energy window above the CBM of $N-Ta_2O_5$. They include the CB edge states and a portion of the quasi-continuous part of DOS in the region where the DOS shows the high-density peak (see Figure 3). The initial excitations to even higher energy levels would be appropriate for modeling intraband relaxation in $N-Ta_2O_5$, rather than for interfacial ET we study.

NA-MD simulation provides the total survival probability for a system to remain in any of the donor states after a time delay, t: $P_{\text{donor}}(t) = \Sigma_{m,n+m\leq 10} P_{n+m}(t)$. The computed probability is averaged over initial excitations to all considered donor states. The wave function isosurfaces of the acceptor and lowest donor states in the COOH and PO_3H_2 system are shown in Figure 4. One can observe a distinct difference in the localization of the orbitals, consistent with an intuitive assumption about the nature of donor and acceptor states. We should note, however, that this localization can become less pronounced as a result of dynamical disorder. One then would observe a notable mixing of the defined donor and acceptor states in instantaneous snapshots. Nonetheless, the distinctive features of the donor and acceptor states remain valid during the course of MD.

3. RESULTS AND DISCUSSION

3.1. Electron Transfer Dynamics. The results of NA-MD calculations are presented in Figure 5. First, we compare the population transfer dynamics without effects of electronic decoherence (Figure 5a). The initial relaxation shows weak Gaussian character, which is typical for quantum processes. The Gaussian component decays when quantum dynamics develops to encompass multiple states. The rest of the relaxation follows the exponential decay law. We determine the ET time to be 530 fs for the COOH system and 5.50 ps for the PO_3H_2 system. The ET occurs on much shorter time scale in the COOH system. In the fully coherent FSSH description, population transfer is governed by NAC and energy gap between donor and acceptor states. The energy gap magnitudes are very similar in the COOH and PO_3H2 systems, as it follows from Table 1. We, therefore, conclude that the major reason leading to very distinct intrinsic efficiencies of the ET in these systems is disparity of the NAC magnitudes.

The fully coherent scheme is known to underestimate transition times of slow processes, because it lacks the important decoherence effects stemming from system-bath interactions.[78,79] The results in Figure 5a are valid only for a hypothetic system, in which the electronic subsystem is isolated from the bath of quantum vibrations. We use it to demonstrate the dominant role of NAC in determining the qualitative trends in ET for complexes attached with different anchors. To obtain quantitative results for transitions happening on picosecond and longer time scales, it is important to include decoherence effects into NA-MD. We utilize the decoherence-induced surface hopping method.[80] The results are presented in Figure 5b.

As expected, nonadiabatic dynamics that includes decoherence shows slower ET. The decay curves follow exponential law with practically absent Gaussian component. The time scales obtained for the COOH and PO_3H_2 systems are 7.50 and 56.7 ps, respectively. The time scale for the COOH system agrees reasonably well with the experimentally measured value of 12 ± 1 ps.[81] The experimentally measured time scale for the PO_3H_2 system is not available. Judging by the results for the COOH

DOI: 10.1021/jacs.5b07454
J. Am. Chem. Soc. 2015, 137, 11517−11525

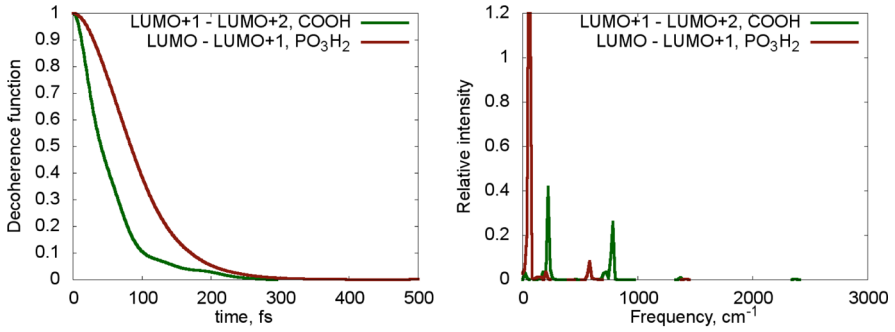

(a) (b)

Figure 7. Decoherence functions (a) and spectral densities (b) of the COOH (green lines) and PO_3H_2 (red lines) systems computed using fluctuation of the gap between appropriate donor and acceptor states.

system, the inclusion of decoherence improves significantly the quantitative accuracy of the computed time scales. The qualitative trend remains similar to the earlier results (Figure 5a). The ET is faster in the system with the COOH anchor. Moreover, the ratio of the ET times changes little, leading to the conclusion that the only role of decoherence is the reduction of the ET rates. Coherence effects do not alter the qualitative trends observed across the different systems. Hence, one expects that the trends can be explained by the NAC magnitudes.

3.2. Role of Nonadiabatic Coupling. As it has been conjectured in the previous section, the NAC should be larger in the COOH system. In order to verify this hypothesis, we compute the 2D maps showing the time-averaged NAC magnitudes for all pairs of orbitals in the considered range (Figure 6). The quantities are computed as $\langle \mathrm{Im}(H_{\mathrm{vib},ij})\rangle = (\hbar/T)\sum_{t=0}^{T-1}|D_{ij}(t)|$, where T is the number of steps in the MD trajectory, t runs over the time steps, and $\langle\rangle$ denotes the time averaging.

The COOH system (Figure 6a) exhibits strong coupling of the LUMO+1 and LUMO+2 levels, with the magnitude of ca. 300 meV. This large coupling realizes an efficient population transfer from the lowest donor (LUMO+2) state to the upper acceptor (LUMO+1) level. One can also observe that there is a secondary channel for the exciton relaxation via a direct coupling between the LUMO+2 state and the LUMO+4−LUMO+6 states. This channel promotes faster electron relaxation to the lowest donor state (LUMO+2), and therefore facilitates the interfacial ET. These couplings are smaller than those between LUMO+1 and LUMO+2, on the order of 20−50 meV, but are still much larger than the couplings with other states, except for couplings between sequential LUMO+n and LUMO+n+1 states. The secondary channel is visualized on the 2D map as green off-diagonal areas. Visualization of the isosurfaces of the LUMO+4, 5, 6 orbitals (see Supporting Information, section B) indicates that the orbitals are mostly localized on the N−Ta_2O_5 cluster, and are partially delocalized to the Ru complex, providing a possible explanation of the notable coupling.

The situation is different for the PO_3H_2 system (Figure 6b). Here, we observe only a single ET channel, between the LUMO acceptor state and the LUMO+1 donor state. Most importantly, the average magnitudes of the couplings are almost an order of magnitude smaller than those in the COOH system. The coupling between LUMO and LUMO+1 is on the order of only 20−30 meV.

The 2D maps clearly show the regions of strong coupling between higher-lying orbitals. As seen in pDOS of Figure 3, states localized on the Ru-complex are in resonance with higher-lying CB states of N−Ta_2O_5. As a result, the orbitals are mixed and strongly coupled to each other. Therefore, a high-energy excitation will lead to fast ET to the Ru complex via these intraband couplings.

It is important to explain the fundamental reasons leading to large NACs in the COOH system compared to those in PO_3H_2. As it follows from the NAC definition, NAC characterizes wave function sensitivity to nuclear motion. One may expect larger couplings for the PO_3H_2 anchor, since the group is more flexible due to sp^3 hybridization of the central P atom, whereas COOH is more rigid due to sp^2 hybridization of the C atom. However, nuclear motion is not the determining factor. pDOS of the COOH system (section B of the Supporting Information) shows that both LUMO and LUMO+1 contain notable contributions from the central C atom of the COOH anchor, because the anchor is conjugated to the ligand π-system. Thus, motion of the COOH group strongly affects the acceptor wave functions and the donor−acceptor NAC. On the contrary, pDOS of the PO_3H_2 system shows little contribution of anchor orbitals to the only acceptor state (LUMO). Therefore, motions of the PO_3H_2 group do not affect the acceptor wave function notably, leading to smaller NAC.

3.3. Role of Quantum Coherence. The role of quantum coherence in natural and artificial light-harvesting is receiving significant attention.[82−89] To fully characterize ET dynamics in the COOH and PO_3H_2 systems, we have analyzed decoherence properties of these complexes. Using the optical response function formalism;[90,91] we compute decoherence functions (Figure 7a). These functions show how quickly electronic coherences are destroyed due to interactions with phonons. Frequent "observation" or "measurement" of the electronic state of the system by the vibrational environment forces the system to collapse onto one of its eigenstates, causing decoherence. Therefore, fast decoherence may "return" the system to its initial electronic state, slowing down electronic transitions. On the contrary, when the system evolves as a coherent superposition of several states, electronic transitions are accelerated. The decoherence function quantifies the rate with which the system looses its memory about the past, and hence shows how frequently the system is "returned" to its original state by the environment-induced fluctuations. We observe that coherence decays faster in the COOH system than

DOI: 10.1021/jacs.5b07454
J. Am. Chem. Soc. 2015, 137, 11517−11525

in the PO_3H_2 system. The computed decoherence times for the two main transitions LUMO+2 → LUMO+1 (in COOH) and LUMO+1 → LUMO (in PO_3H_2) are ca. 30 and 105 fs, respectively.

The observed trends in both NAC and decoherence are caused by the same factors, namely, anchor motions and delocalization of donor and acceptor orbitals onto anchor. One may assume that the COOH anchor, being a planar and more rigid than the PO_3H_2, can induce smaller structural fluctuations than the more flexible PO_3H_2 group. In our previous study,[44] we found that the fluctuation of the tilt angle of these Ru complexes relative to the substrate plane are, in fact, comparable to each other. The structural fluctuation analysis suggests that there would be no notable difference in decoherence times due to differences in motion of the two complexes.

The structural dynamics is not the direct factor that affects decoherence times. Similar to our analysis of NAC in their relation to orbital-resolved pDOS, it is the response of the energy gap fluctuation to the structural changes that matters the most. There are situations when structural correlations may decay very rapidly, whereas coherence can still persist for a long time.[92] To understand the origins of faster decoherence in the COOH system, we analyze the autocorrelation function (ACF) of the energy gap fluctuation, $\langle \delta E_{AD}(0)\, \delta E_{AD}(t)\rangle$, where A and D denote the acceptor and donor states, respectively. The Fourier transform of the ACF reveals the frequencies of the gap fluctuation (Figure 7b). Generally, the higher the frequency of such fluctuations, the faster the decoherence, because the wave functions corresponding to the two energy levels would build up a larger phase difference.

The results shown in Figure 7b indicate that the donor−acceptor energy gap fluctuation occurs with a smaller frequency in the PO_3H_2 system than in the COOH. In accord with our explanation above, this result suggests that decoherence in the COOH occurs faster than in the PO_3H_2 system. The atomistic origins for this effect are twofold. First, the LUMO state in the PO_3H_2 system does not have any notable contribution of anchor orbitals. Thus, motion of the PO_3H_2 anchor does not affect the orbital energies as much as motion of the COOH anchor does. We observe the same reason that made NAC smaller in the PO_3H_2 system than in the COOH complex. Second, the vibrations of the aromatic C−C bond connecting the Ru complex and the COOH anchor are faster than the vibrations of the analogous aliphatic P−C bond in the PO_3H_2 system: both because of a larger force constant for the C−C bond as compared to the P−C bond, and due to a smaller atomic mass of the C atom as compared to the P atom. The faster vibration leads to a more rapid evolution of the wave function phase for each energy level, and to faster accumulation of the phase difference for the energy level pair.

Faster decoherence in the COOH system should decelerate ET more than in the PO_3H_2 complex. This effect is achieved in our simulations, indeed: the deceleration ratio for the COOH can be defined as $dr_{COOH} = \tau_{decoherence}(COOH)/\tau_{no\text{-}decoherence}(COOH) = 14.15$, the analogously defined deceleration ratio for the PO_3H_2 system is $dr_{PO_3H_2} = 10.31$. Inclusion of decoherence favors faster dynamics in the PO_3H_2 system. However, the effect is relatively small. On the other hand, the effects due to differences in NACs are significantly more pronounced: the ratio of the averaged NACs between the donor and acceptor levels of the two systems reaches the order of 10. Overall, ET is notably faster in the COOH system.

3.4. Implications to the ET in the COOH and PO_3H_2 Systems. The conclusions from our calculations are in formal contrast with the previous experimental measurements,[43] which report an opposite trend: Our calculations predict the COOH anchor to be more efficient than PO_3H_2, whereas the experimental TONs are larger for the PO_3H_2 system. Our results address only one factor affecting the overall efficiency of the photocatalytic CO_2 reduction. Structure of the catalyst surface is the most likely reason for the discrepancy. It has been known from other studies that molecules attached via the COOH anchor are very sensitive to conditions such as pH and solvent.[25,26] It is easier for the system with the COOH anchor to detach from the substrate, partially because the final anion forms an extended aromatic system, stabilizing the dissociation product. There is no such stabilization for the PO_3H_2 anchor. The PO_3H_2 system is more stable,[24,25] leading to a larger surface coverage and, hence, higher TONs. Finally, the reduction potential of CO_2 is greater than that of almost any other organic system found in a photocatalytic cell. The electron injected into the Ru complex can reduce the COOH group. We attribute the larger TONs observed experimentally in the PO_3H_2 system to higher stability and effective surface coverage, and to smaller extent of self-reduction.

Very recently, Sato et al. synthesized the electroneutral COOH and PO_3H_2 systems, and evaluated their photocatalytic activities.[93] Contrary to the previously reported results for $[Ru(dcbpy)\ (bpy)\ (CO)_2]^{2+}$ and $[Ru(dpbpy)\ (bpy)\ (CO)_2]^{2+}$, they found that an initial TON of CO_2 reduction using $[Ru(dcbpy)\ (CO)_2Cl_2]$ was about three times larger than that using $[Ru(dpbpy)\ (CO)_2Cl_2]$, which is consistent with the present theoretical prediction. In addition, they observed that the COOH system was deactivated after 15 h, suggesting instability of the catalyst surface.

Intrinsic properties of the COOH anchor suggest that the complexes attached with this group should be more efficient in an ideal environment. This conclusion agrees with other simulations[31] that report faster ET in systems attached with the COOH anchor compared to the PO_3H_2 anchor. Additional evidence supporting our conclusion can be inferred from the existing experimental works. For example, Mulhern et al.[94] showed that electrons are injected approximately twice as efficiently from chalcogenorhodamine dyes anchored to TiO_2 via carboxylate linkages than via phosphonate linkages. Bae et al.[25] reported larger steady-state photocurrents in RuL_3 complexes attached to TiO_2 with the COOH anchor as opposed to the analogous molecules attached with the PO_3H_2 anchor. The photocurrent can be linked to ET rates directly, whereas TONs values can be affected by the surface coverage and other factors. Higher stability of the PO_3H_2 anchor in contrast to that of COOH is also suggested by the direct calculations of the binding energy, although the effect may depend on the choice of the surface plane.[95]

4. CONCLUSIONS

We have reported nonadiabatic dynamics studies of ET in the prototypical $Ru(di\text{-}X\text{-}bpy)\ (CO)_2Cl_2/N{-}Ta_2O_5$ complexes for photocatalytic CO_2 reduction. We have investigated the role the anchor groups, X = COOH and PO_3H_2, play in determining the efficiencies of these systems. Our calculations show notably faster ET in the COOH system compared to PO_3H_2. The computed ET time scales in the COOH and

DOI: 10.1021/jacs.5b07454
J. Am. Chem. Soc. 2015, 137, 11517−11525

PO_3H_2 systems are 7.50 and 56.7 ps, respectively. The ET time scale in the COOH system is in good agreement with the experimentally measured value of 12 ± 1 ps. We attribute the observed difference of the ET times in the two systems to a significant difference in the magnitudes of NAC, which on average are equal to 300 meV and 20−30 meV for COOH and PO_3H_2, respectively.

Quantum coherence counteracts NAC; however, NAC plays a more important role. Electronic decoherence in the COOH system is faster than that in PO_3H_2, 30 and 105 fs, respectively. Overall, decoherence slows down ET by an order of magnitude. At the same time, it decelerates ET only slightly more in the COOH complex than in the PO_3H_2 complex, having only a small effect on the ratio of the ET times in the two systems.

The observed trends in the NAC and decoherence rates are both explained by sensitivity of the acceptor state wave functions to motion of the anchor groups. This sensitivity is analyzed using orbital-resolved pDOS. The frontier level of the PO_3H_2 system contains no contribution from the anchor. On the contrary, the acceptor states in the COOH system contain a notable fraction of orbitals of the C atom of the COOH anchor group, leading to larger NAC and smaller decoherence times.

The results of our calculations indicate that the COOH anchor is intrinsically more efficient than PO_3H_2. This conclusion is supported by the existing computational and experimental studies for similar systems. We argue that our computationally efficient method is capable of capturing important qualitative trends, despite the method's simplicity. We expect the qualitative conclusions to hold for more elaborate methodologies.

We suggest that the experimentally observed TONs are not necessarily indicative of faster or slower ET dynamics at the semiconductor/Ru-complex interface. Other factors are likely to play a notable role. Existing experimental data indicate that effective surface coverage may be one of such factors. The coverage in the COOH system is likely to be lower due dissociation of the anchor-surface bond and reduction of the COOH anchor by the photogenerated charges. The possibility of the latter process is supported by our electronic structure calculations, showing a notable localization of the acceptor state electron density on COOH. The reported comprehensive, time-domain, atomistic analysis of the photoinduced dynamics establishes the fundamental ET mechanisms and highlights the importance of anchor stability, nonadiabatic transitions and quantum coherence in artificial photocatalysis

■ ASSOCIATED CONTENT

Supporting Information

The Supporting Information is available free of charge on the ACS Publications website at DOI: 10.1021/jacs.5b07454.

Optimized EHT parameters and orbital-resolved pDOSs (PDF)

Geometry of COOH system (XYZ)

Geometry of PO_3H_2 system (XYZ)

■ AUTHOR INFORMATION

Corresponding Author

*prezhdo@usc.edu

Notes

The authors declare no competing financial interest.

■ ACKNOWLEDGMENTS

A.V.A and O.V.P. acknowledge financial support of the U.S. Department of Energy, Grant DE-SC0014429. We also thank T. Morikawa, S. Sato, and T. Suzuki for their fruitful discussions. R.A. and R.J. acknowledge partial financial support from Advanced Catalytic Transformation Program for Carbon Utilization (ACT-C) supported by Japan Science and Technology Agency (JST).

■ REFERENCES

(1) Gust, D.; Moore, T. A.; Moore, A. L. *Acc. Chem. Res.* **2009**, *42* (12), 1890−1898.

(2) Yadav, R. K.; Baeg, J.-O.; Oh, G. H.; Park, N.-J.; Kong, K.; Kim, J.; Hwang, D. W.; Biswas, S. K. *J. Am. Chem. Soc.* **2012**, *134* (28), 11455−11461.

(3) Kärkäs, M. D.; Johnston, E. V.; Verho, O.; Åkermark, B. *Acc. Chem. Res.* **2014**, *47* (1), 100−111.

(4) Styring, S. *Faraday Discuss.* **2012**, *155*, 357−376.

(5) Noji, T.; Suzuki, H.; Gotoh, T.; Iwai, M.; Ikeuchi, M.; Tomo, T.; Noguchi, T. *J. Phys. Chem. Lett.* **2011**, *2* (19), 2448−2452.

(6) Pei, D.; Luan, J. *Int. J. Photoenergy* **2012**, *2012*, 262831.

(7) Li, H.; Li, F.; Zhang, B.; Zhou, X.; Yu, F.; Sun, L. *J. Am. Chem. Soc.* **2015**, *137* (13), 4332−4335.

(8) Procacci, B.; Jiao, Y.; Evans, M. E.; Jones, W. D.; Perutz, R. N.; Whitwood, A. C. *J. Am. Chem. Soc.* **2015**, *137* (3), 1258−1272.

(9) McCrory, C. C. L.; Jung, S.; Ferrer, I. M.; Chatman, S. M.; Peters, J. C.; Jaramillo, T. F. *J. Am. Chem. Soc.* **2015**, *137* (13), 4347−4357.

(10) Jiao, Y.; Morris, J.; Brennessel, W. W.; Jones, W. D. *J. Am. Chem. Soc.* **2013**, *135* (43), 16198−16212.

(11) Gao, Y.; Ding, X.; Liu, J.; Wang, L.; Lu, Z.; Li, L.; Sun, L. *J. Am. Chem. Soc.* **2013**, *135* (11), 4219−4222.

(12) Iwase, A.; Ng, Y. H.; Ishiguro, Y.; Kudo, A.; Amal, R. *J. Am. Chem. Soc.* **2011**, *133* (29), 11054−11057.

(13) Kudo, A.; Miseki, Y. *Chem. Soc. Rev.* **2009**, *38* (1), 253−278.

(14) Walter, M. G.; Warren, E. L.; McKone, J. R.; Boettcher, S. W.; Mi, Q.; Santori, E. A.; Lewis, N. S. *Chem. Rev.* **2010**, *110* (11), 6446−6473.

(15) Grills, D. C.; Fujita, E. *J. Phys. Chem. Lett.* **2010**, *1* (18), 2709−2718.

(16) Mikkelsen, M.; Jørgensen, M.; Krebs, F. C. *Energy Environ. Sci.* **2010**, *3* (1), 43.

(17) Joshi, U. A.; Palasyuk, A.; Arney, D.; Maggard, P. A. *J. Phys. Chem. Lett.* **2010**, *1* (18), 2719−2726.

(18) Markewitz, P.; Kuckshinrichs, W.; Leitner, W.; Linssen, J.; Zapp, P.; Bongartz, R.; Schreiber, A.; Müller, T. E. *Energy Environ. Sci.* **2012**, *5* (6), 7281.

(19) Kobayashi, K.; Tanaka, K. *Phys. Chem. Chem. Phys.* **2014**, *16* (6), 2240−2250.

(20) Arai, T.; Sato, S.; Kajino, T.; Morikawa, T. *Energy Environ. Sci.* **2013**, *6* (4), 1274.

(21) Takeda, H.; Koizumi, H.; Okamoto, K.; Ishitani, O. *Chem. Commun.* **2014**, *50* (12), 1491−1493.

(22) Fu, Y.; Sun, D.; Chen, Y.; Huang, R.; Ding, Z.; Fu, X.; Li, Z. *Angew. Chem.* **2012**, *124* (14), 3420−3423.

(23) Tamaki, Y.; Morimoto, T.; Koike, K.; Ishitani, O. *Proc. Natl. Acad. Sci. U. S. A.* **2012**, *109* (39), 15673−15678.

(24) Trammell, S. A.; Moss, J. A.; Yang, J. C.; Nakhle, B. M.; Slate, C. A.; Odobel, F.; Sykora, M.; Erickson, B. W.; Meyer, T. J. *Inorg. Chem.* **1999**, *38* (16), 3665−3669.

(25) Bae, E.; Choi, W.; Park, J.; Shin, H. S.; Kim, S. B.; Lee, J. S. *J. Phys. Chem. B* **2004**, *108* (37), 14093−14101.

(26) McNamara, W. R.; Milot, R. L.; Song, H.; Snoeberger, R. C., III; Batista, V. S.; Schmuttenmaer, C. A.; Brudvig, G. W.; Crabtree, R. H. *Energy Environ. Sci.* **2010**, *3*, 917−923.

(27) McNamara, W. R.; Snoeberger, R. C.; Li, G.; Schleicher, J. M.; Cady, C. W.; Poyatos, M.; Schmuttenmaer, C. A.; Crabtree, R. H.; Brudvig, G. W.; Batista, V. S. *J. Am. Chem. Soc.* **2008**, *130* (43), 14329−14338.

(28) Ambrosio, F.; Martsinovich, N.; Troisi, A. *J. Phys. Chem. Lett.* **2012**, *3* (11), 1531−1535.
(29) Ambrosio, F.; Martsinovich, N.; Troisi, A. *J. Phys. Chem. C* **2012**, *116* (3), 2622−2629.
(30) Martsinovich, N.; Troisi, A. *J. Phys. Chem. C* **2011**, *115*, 11781−11792.
(31) Wang, L.; Ernstorfer, R.; Willig, F.; May, V. *J. Phys. Chem. B* **2005**, *109* (19), 9589−9595.
(32) Wang, L.; Willig, F.; May, V. *J. Chem. Phys.* **2006**, *124* (1), 014712.
(33) Stern, C.; Bessmertnykh Lemeune, A.; Gorbunova, Y.; Tsivadze, A.; Guilard, R. *Turk. J. Chem.* **2014**, *38*, 980−993.
(34) Youngblood, W. J.; Lee, S.-H. A.; Maeda, K.; Mallouk, T. E. *Acc. Chem. Res.* **2009**, *42* (12), 1966−1973.
(35) Youngblood, W. J.; Lee, S.-H. A.; Kobayashi, Y.; Hernandez-Pagan, E. A.; Hoertz, P. G.; Moore, T. A.; Moore, A. L.; Gust, D.; Mallouk, T. E. *J. Am. Chem. Soc.* **2009**, *131* (3), 926−927.
(36) Swierk, J. R.; McCool, N. S.; Saunders, T. P.; Barber, G. D.; Mallouk, T. E. *J. Am. Chem. Soc.* **2014**, *136* (31), 10974−10982.
(37) Sauvage, F.; Chhor, S.; Marchioro, A.; Moser, J.-E.; Graetzel, M. *J. Am. Chem. Soc.* **2011**, *133* (33), 13103−13109.
(38) Jakubikova, E.; Snoeberger, R. C., III; Batista, V. S.; Martin, R. L.; Batista, E. R. *J. Phys. Chem. A* **2009**, *113* (45), 12532−12540.
(39) Guo, J.; Stockwell, D.; Ai, X.; She, C.; Anderson, N. A.; Lian, T. *J. Phys. Chem. B* **2006**, *110* (11), 5238−5244.
(40) Wenger, B.; Grätzel, M.; Moser, J.-E. *J. Am. Chem. Soc.* **2005**, *127* (35), 12150−12151.
(41) Sato, S.; Morikawa, T.; Saeki, S.; Kajino, T.; Motohiro, T. *Angew. Chem., Int. Ed.* **2010**, *49* (30), 5101−5105.
(42) Sato, S.; Arai, T.; Morikawa, T.; Uemura, K.; Suzuki, T. M.; Tanaka, H.; Kajino, T. *J. Am. Chem. Soc.* **2011**, *133* (39), 15240−15243.
(43) Suzuki, T. M.; Tanaka, H.; Morikawa, T.; Iwaki, M.; Sato, S.; Saeki, S.; Inoue, M.; Kajino, T.; Motohiro, T. *Chem. Commun.* **2011**, *47* (30), 8673.
(44) Akimov, A. V.; Jinnouchi, R.; Asahi, R.; Prezhdo, O. V. *J. Phys. Chem. B* **2015**, *119*, 7186−7197.
(45) Jinnouchi, R.; Akimov, A. V.; Shirai, S.; Asahi, R.; Prezhdo, O. V. *J. Phys. Chem. C*, in preparation .
(46) Morikawa, T.; Saeki, S.; Suzuki, T.; Kajino, T.; Motohiro, T. *Appl. Phys. Lett.* **2010**, *96* (14), 142111.
(47) Akimov, A. V.; Kolomeisky, A. B. *J. Chem. Theory Comput.* **2011**, *7*, 3062−3071.
(48) Rappe, A. K.; Casewit, C. J.; Colwell, K. S.; Goddard, W. A., III; Skiff, W. M. *J. Am. Chem. Soc.* **1992**, *114* (25), 10024−10035.
(49) Nose, S. *J. Chem. Phys.* **1984**, *81* (1), 511−519.
(50) Hoover, W. G. *Mol. Simul.* **2007**, *33* (1−2), 13−19.
(51) Hoffmann, R. *J. Chem. Phys.* **1963**, *39* (6), 1397−1412.
(52) Hoffmann, R. *J. Chem. Phys.* **1964**, *40* (9), 2745−2745.
(53) Hoffmann, R. *J. Chem. Phys.* **1964**, *40* (9), 2474−2480.
(54) Amouyal, E.; Mouallem-Bahout, M.; Calzaferri, G. *J. Phys. Chem.* **1991**, *95* (20), 7641−7649.
(55) Cerda, J.; Soria, F. *Phys. Rev. B: Condens. Matter Mater. Phys.* **2000**, *61* (12), 7965−7971.
(56) Abuabara, S. G.; Rego, L. G. C.; Batista, V. S. *J. Am. Chem. Soc.* **2005**, *127* (51), 18234−18242.
(57) da Silva, R.; Rego, L. G. C.; Freire, J. A.; Rodriguez, J.; Laria, D.; Batista, V. S. *J. Phys. Chem. C* **2010**, *114* (45), 19433−19442.
(58) Hoffmann, R. *Rev. Mod. Phys.* **1988**, *60* (3), 601−628.
(59) Negre, C. F. A.; Young, K. J.; Oviedo, M. B.; Allen, L. J.; Sánchez, C. G.; Jarzembska, K. N.; Benedict, J. B.; Crabtree, R. H.; Coppens, P.; Brudvig, G. W.; Batista, V. S. *J. Am. Chem. Soc.* **2014**, *136* (46), 16420−16429.
(60) Li, C.; Koenigsmann, C.; Ding, W.; Rudshteyn, B.; Yang, K. R.; Regan, K. P.; Konezny, S. J.; Batista, V. S.; Brudvig, G. W.; Schmuttenmaer, C. A.; Kim, J.-H. *J. Am. Chem. Soc.* **2015**, *137* (4), 1520−1529.
(61) Voityuk, A. A. *J. Chem. Theory Comput.* **2008**, *4* (11), 1877−1885.
(62) Voityuk, A. A. *J. Chem. Theory Comput.* **2006**, *2* (4), 1038−1044.
(63) Rego, L. G. C.; Hames, B. C.; Mazon, K. T.; Joswig, J.-O. *J. Phys. Chem. C* **2014**, *118* (1), 126−134.
(64) Rego, L. G. C.; Abuabara, S. G.; Batista, V. S. *J. Chem. Phys.* **2005**, *122* (15), 154709.
(65) Iron, M. A.; Heyden, A.; Staszewska, G.; Truhlar, D. G. *J. Chem. Theory Comput.* **2008**, *4* (5), 804−818.
(66) Akimov, A. V.; Prezhdo, O. V. *J. Math. Chem.* **2015**, *53*, 528−550.
(67) Kalman, B. L. *J. Chem. Phys.* **1973**, *59* (9), 5184−5188.
(68) Wang, Y.; Nordlander, P.; Tolk, N. H. *J. Chem. Phys.* **1988**, *89* (7), 4163−4169.
(69) Kitamura, M.; Inoue, K.; Chen, H. *Mater. Chem. Phys.* **2000**, *62* (2), 122−130.
(70) Akimov, A. V.; Prezhdo, O. V. *J. Chem. Theory Comput.* **2013**, *9*, 4959−4972.
(71) Akimov, A. V.; Prezhdo, O. V. *J. Chem. Theory Comput.* **2014**, *10* (2), 789−804.
(72) Tully, J. C. *J. Chem. Phys.* **1990**, *93* (2), 1061−1071.
(73) Hack, M. D.; Truhlar, D. G. *J. Phys. Chem. A* **2000**, *104* (34), 7917−7926.
(74) Hack, M. D.; Wensmann, A. M.; Truhlar, D. G.; Ben-Nun, M.; Martínez, T. J. *J. Chem. Phys.* **2001**, *115* (3), 1172.
(75) Drukker, K. *J. Comput. Phys.* **1999**, *153*, 225−272.
(76) Akimov, A. V.; Neukirch, A. J.; Prezhdo, O. V. *Chem. Rev.* **2013**, *113*, 4496−4565.
(77) Wang, L.; Long, R.; Prezhdo, O. V. *Annu. Rev. Phys. Chem.* **2015**, *66* (1), 549−579.
(78) Prezhdo, O. V.; Rossky, P. J. *J. Chem. Phys.* **1997**, *107* (15), 5863−5878.
(79) Landry, B. R.; Subotnik, J. E. *J. Chem. Phys.* **2011**, *135* (19), 191101−191101.
(80) Jaeger, H. M.; Fischer, S.; Prezhdo, O. V. *J. Chem. Phys.* **2012**, *137*, 22A545.
(81) Yamanaka, K.; Sato, S.; Iwaki, M.; Kajino, T.; Morikawa, T. *J. Phys. Chem. C* **2011**, *115* (37), 18348−18353.
(82) Fuller, F. D.; Pan, J.; Gelzinis, A.; Butkus, V.; Senlik, S. S.; Wilcox, D. E.; Yocum, C. F.; Valkunas, L.; Abramavicius, D.; Ogilvie, J. P. *Nat. Chem.* **2014**, *6*, 706.
(83) Fidler, A. F.; Singh, V. P.; Long, P. D.; Dahlberg, P. D.; Engel, G. S. *J. Phys. Chem. Lett.* **2013**, *4* (9), 1404−1409.
(84) Kolli, A.; O'Reilly, E. J.; Scholes, G. D.; Olaya-Castro, A. *J. Chem. Phys.* **2012**, *137* (17), 174109.
(85) Hayes, D.; Griffin, G. B.; Engel, G. S. *Science* **2013**, *340* (6139), 1431−1434.
(86) Hayes, D.; Griffin, G. B.; Engel, G. S. *Science* **2014**, *344* (6188), 1099−1099.
(87) Pachón, L. A.; Brumer, P. *J. Phys. Chem. Lett.* **2011**, *2* (21), 2728−2732.
(88) Strümpfer, J.; Şener, M.; Schulten, K. *J. Phys. Chem. Lett.* **2012**, *3* (4), 536−542.
(89) Kassal, I.; Yuen-Zhou, J.; Rahimi-Keshari, S. *J. Phys. Chem. Lett.* **2013**, *4* (3), 362−367.
(90) Mukamel, S. *Principles of Nonlinear Optical Spectroscopy*; Oxford University Press: New York, 1995.
(91) Madrid, A. B.; Hyeon-Deuk, K.; Habenicht, B. F.; Prezhdo, O. V. *ACS Nano* **2009**, *3* (9), 2487−2494.
(92) Akimov, A. V.; Prezhdo, O. V. *J. Phys. Chem. Lett.* **2013**, *4* (22), 3857−3864.
(93) Sato, S.; Morikawa, T. In preparation.
(94) Mulhern, K. R.; Detty, M. R.; Watson, D. F. *J. Photochem. Photobiol., A* **2013**, *264*, 18−25.
(95) O'Rourke, C.; Bowler, D. R. *J. Phys.: Condens. Matter* **2014**, *26* (19), 195302.

DOI: 10.1021/jacs.5b07454
J. Am. Chem. Soc. 2015, 137, 11517−11525